MINIREVIEW

Check for updates

Recent research progress on building C–N bonds *via* electrochemical NO$_x$ reduction

Shaktiswaran R. Udayasurian (ID) and Tengfei Li (ID)*

The release of NO$_x$ species (such as nitrate, nitrite and nitric oxide) into water and the atmosphere due to human being's agricultural and industrial activities has caused a series of environmental problems, including accumulation of toxic pollutants that are dangerous to humans and animals, acid rain, the greenhouse effect and disturbance of the global nitrogen cycle balance. Electrosynthesis of organonitrogen compounds with NO$_x$ species as the nitrogen source offers a sustainable strategy to upgrade the waste NO$_x$ into value-added organic products under ambient conditions. The electrochemical reduction of NO$_x$ species can generate surface-adsorbed intermediates such as hydroxylamine, which are usually strong nucleophiles and can undergo nucleophilic attack to carbonyl groups to build C–N bonds and generate organonitrogen compounds such as amine, oxime, amide and amino acid. This mini-review summarizes the most recent progress in building C–N bonds *via* the *in situ* generation of nucleophilic intermediates from electrochemical NO$_x$ reduction, and highlights some important strategies in facilitating the reaction rates and selectivities towards the C–N coupling products. In particular, the preparation of high-performance electrocatalysts (*e.g.*, nano-/atomic-scale catalysts, single-atom catalysts, alloy catalysts), selection of nucleophilic intermediates, novel design of reactors and understanding the surface adsorption process are highlighted. A few key challenges and knowledge gaps are discussed, and some promising research directions are also proposed for future advances in electrochemical C–N coupling.

School of Chemistry and Environment, Manchester Metropolitan University, Chester Street, Manchester, M1 5GD, UK. E-mail: t.li@mmu.ac.uk

Shaktiswaran R. Udayasurian

Shaktiswaran is currently a PhD student at Manchester Metropolitan University under the supervision of Dr Tengfei Li, specializing in the design of electrocatalysts for the electrocatalytic conversion of nitrate, ammonia and CO$_2$. He received his MEng in Materials Science and Engineering with Corrosion from University of Manchester in 2019. He received his MSc in Data Science and Artificial Intelligence from Goldsmiths, University of London in 2020. Previously, he was a research assistant at Agency for Science, Technology and Research Institute of High-Performance Computing and Nanyang Technological University, Singapore from 2020 to 2022.

1. Introduction

The global environmental and energy crisis due to the combustion of fossil fuels demands a transition in the synthetic industry from dependence on fossil fuels to sustainable energy, *e.g.*, renewable electricity.[1,2] Organic electrosynthesis has emerged as a promising strategy as it can enable ambient reaction conditions and drive redox reactions by clean electrons instead of toxic or expensive chemical reagents.[3–5] Electrochemical upgrading of pollutants and greenhouse gases into value-added organic products is particularly attractive, because it can not only be driven by clean electricity, but also utilize the environmentally unfriendly wastes as the feedstocks for synthesis.[6–8]

The emission of NO$_x$ species, such as nitrate (NO$_3^-$), nitrite (NO$_2^-$), nitric oxide (NO) and nitrogen dioxide (NO$_2$), has become a serious environmental challenge. For example, the accumulation of NO$_3^-$ in water due to excessive fertiliser usage and industrial sewage has disturbed the global nitrogen cycle balance.[9–11] Although NO$_3^-$ itself is not dangerous to human beings, NO$_3^-$ can be easily reduced to NO$_2^-$, which is toxic as it can cause damages of red blood cells.[9] Furthermore, the emission of gaseous nitrogen oxide compounds has also significantly contributed to the global warming effect: the greenhouse effect of N$_2$O is 265 times that of CO$_2$.[12] On the other

side, organonitrogen compounds, such as urea, amide, amino acid and oxime, are very important in agricultures and polymer and pharmaceutical industries. Therefore, it is desirable to upgrade waste NO_x species into value-added organonitrogen compounds, which can enable the removal of environmental pollutants and the synthesis of high-value products simultaneously.

Electrochemical NO_x reduction reaction (NO_xRR) offers a sustainable method to convert the NO_x species into ammonia (NH_3).[13–30] Compared to the electrochemical reduction of N_2 into NH_3, NO_xRR can utilize the activated N species in environment and avoid the requirement of breaking the stable N≡N bond, and thus can make NH_3 at higher faradaic efficiency (FE) and current density. The state-of-the-arts NO_xRR systems can produce NH_3 with ~90% FE at ~1 A cm^{-2}.[31–34] Although NH_3 is a very important chemical building block, it is still desirable to make nitrogen products via electrochemical NO_xRR that bear higher economic values than NH_3, such as organonitrogen compounds.

Recently, a series of surface-adsorbed reaction intermediates have been identified in the electrochemical NO_xRR process, such as *NH_2OH and *NH_2. These intermediates are typically stronger nucleophiles compared to the final product of NO_xRR (i.e., NH_3), and therefore can be coupled with chemical reactions and undergo nucleophilic attack to carbonyl species (e.g. ketone, aldehyde, CO_2, CO) to build C–N bonds in a wide range of organic products (Fig. 1). These C–N coupling reactions are usually more difficult to occur between NH_3 and the carbonyl species (i.e. typically require high temperatures/pressures).[35] Furthermore, these highly active N-containing intermediates are unstable over long period of time. For example, the transportation and storage of concentrated NH_2OH are challenged by the risk of explosion.[36] Therefore, the electrochemical NO_xRR also enables an in situ generation of nucleophilic N species on demand for the C–N coupling reaction. Moreover, compared to the traditional chemical methods, the electrosynthesis of organonitrogen compounds
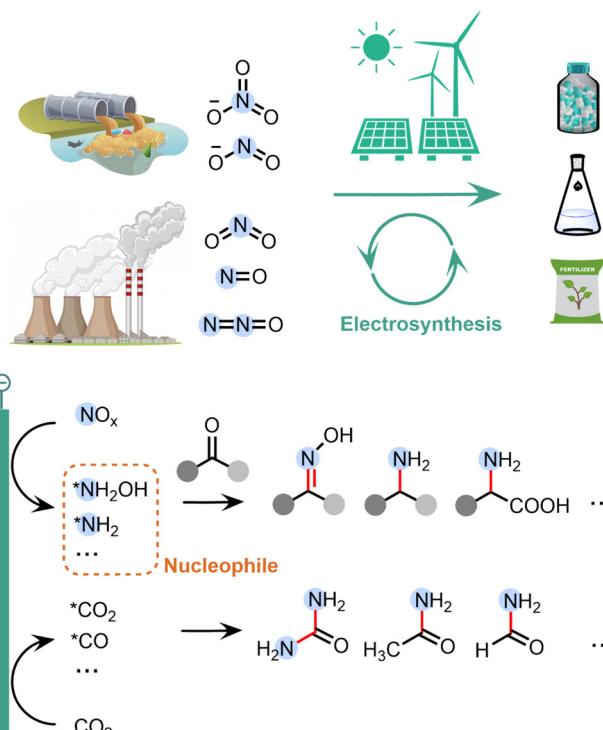

Fig. 1 Electrosynthesis of value-added organonitrogen products from gas- and liquid-phase NO_x compounds. The electroreduction of NO_x can generate a reaction intermediate that can undergo nucleophilic attack to a carbonyl group, including organic ketone/aldehyde and CO_2 reduction intermediates.

via NO_xRR offers a more sustainable synthesis strategy, as it can be performed under ambient conditions (e.g. room temperature and pressure, aqueous media, without expensive or toxic catalyst) and can be coupled with clean electrons to replace redox reagents.

However, building organic C–N bonds by electrochemical NO_xRR is challenged by the generation of a series of by-products, such as N_2, NH_3 and H_2, as well as the hydrogenation products of the organic species, which all decrease the selectivity towards the desired C–N coupling products. In this minireview, we will highlight some emerging strategies to facilitate the electrochemical C–N bond formation via NO_xRR, such as choosing a suitable nucleophile for C–N coupling, tuning the composition and morphology of the electrocatalysts, making catalysts with nano-/atomic-scale and single-atom structures, designing novel reactors, and controlling surface adsorption by understanding the reaction mechanism, etc. As this area is developing quite rapidly, this minireview does not aim to provide a complete compilation of publications (readers may refer to other reviews to get a comprehensive understanding of this area).[37,38] Instead, we will first give a brief summary of building C–N bonds by electrochemical NO_xRR, and then mainly focus the most recent reports in this area in the last two years, and summarize the main challenges and emerging opportunities to develop more efficient NO_xRR systems to drive electrosynthesis of organonitrogen compounds.

Tengfei Li

Dr Tengfei Li is a Senior Lecturer in Chemistry at Manchester Metropolitan University in the UK. He obtained his PhD degree in Chemistry with Prof. Curtis Berlinguette at the University of British Columbia, Canada. He then moved to the University of Cambridge and joined Prof. Erwin Reisner's lab as a Canadian Banting Postdoc Fellow. His independent lab is currently focused on sustainable electrocatalysis and photocatalysis, including organic electrosynthesis, nitrate reduction, CO_2 reduction and plastic degradation.

2. Electrochemical C–N bond formation systems

2.1. Initial explorations on electrochemical C–N coupling: which N species should be used to undergo nucleophilic attack to carbonyl species?

The first electrocatalytic C–N coupling process was demonstrated in 2019 by Jiao's group.[39] During the electrochemical reduction of CO on a commercial-available Cu nanoparticle electrocatalyst, NH_3 was added into the electrolyte, which can undergo a C–N coupling reaction to produce acetamide with a FE of ~40% at 300 mA cm^{-2} and an operating potential at -0.68 V vs. reversible hydrogen electrode (V_{RHE}). The mechanistic study showed that the C–N coupling process occurs through the nucleophilic attack of NH_3 to the $*C{=}C{=}O$ intermediate generated in CO electroreduction to make acetamide, which is in competition with the nucleophilic attack of OH^- to the same intermediate to generate acetate (Fig. 2a). This strategy can be extended to produce other amide compounds by co-electrolysis of CO with different amines, and an increase for the selectivity towards amide was observed when the nucleophilicity of the N species increased, i.e., NH_3 < CH_3NH_2 < $CH_3CH_2NH_2$ < $(CH_3)_2NH$ (Fig. 2b). It is also notable that adding NH_3 into the electrolysis of CO_2 (instead of CO) did not generate any amide. Later Kornienko et al. showed that the co-electrolysis of NH_3 and CO_2 can generate a small amount of formamide and acetamide (FE = 0.4% and 10%, respectively).[40] These results proved the importance of choosing a suitable nucleophile (i.e., N species) and electrophile (i.e., carbonyl species) with high reactivities for the C–N coupling reaction.

In order to increase the nucleophilicity of the N species, different N sources have been investigated for electrochemical C–N bond formation, including NH_3, N_2, and NO_x species. The intermediates generated in electrochemical NO_xRR, such as $*NH_2OH$ and $*NH_2$, are particularly attractive as they are more nucleophilic than NH_3. One of the first successful C–N coupling reactions via electrochemical NO_xRR was reported in 2021 by Wang and coworkers,[41] where the co-reduction of CO_2 and NO_3^- on a cobalt molecule catalyst (CoPc–NH_2, previously reported to drive CO_2RR to methanol by the same group[44]) can generate methylamine (CH_3NH_2) with a FE of 13% at ~25 mA cm^{-2} and an operating potential of $-0.92V_{RHE}$. The key C–N bond formation step was found to be the nucleophilic addition–elimination reaction between the NH_2OH intermediate generated by NO_xRR and the formaldehyde (HCHO) intermediate generated by CO_2 reduction reaction (CO_2RR) to form formaldoxime ($H_2C{=}NOH$), which is then further reduced to CH_3NH_2 (Fig. 2c). Later, Wang's group also investigated coupling CO_2RR with different N nucleophiles (e.g., NH_2OH, NH_2NH_2, primary and secondary amines) and demonstrated that the C–N coupling efficiency was mainly determined by the nucleophilicity of the N species (Fig. 2d).[42] These works highlighted that the in situ generated $*NH_2OH$ in NO_xRR process is a promising nucleophile to build C–N bond, which can be used to make a wide range of organonitrogen compounds (e.g.,

amine, oxime, amino acid) in following works as described in section 2.2.

Another important organonitrogen compound that can be produced by electrochemical NO_xRR is urea, which accounts for two thirds of the global fertilizer market. Urea is mainly produced via the Bosch–Meiser process from CO_2 and NH_3, which requires harsh reaction conditions and is energy intensive (150–200 °C, 150–250 bar, 7.1 GJ per ton).[35] Electrochemical co-reduction of CO_2 and NO_x can provide an alternative method to produce urea under ambient conditions. In 2021, Yu et al. reported that CO_2 and NO_3^- can be reduced by a single-crystal-facet $In(OH)_3$ electrocatalyst to make urea with a FE of 53% at 0.6 mA cm^{-2} and $-0.6V_{RHE}$ (Fig. 2e).[43] Despite of the relatively low current density, the nitrogen and carbon selectivities towards urea are high (83% and 100%, respectively), which are quite remarkable considering that NO_xRR and CO_2RR can usually generate a series of by-products such as NH_3, N_2, CO and formate. The high selectivities were attributed to the low energy barrier for the C–N coupling step on the (100) facets of the $In(OH)_3$ catalyst. The single-crystal-facet $In(OH)_3$ electrocatalyst with well-defined (100) facets via a reported solvothermal approach[45] (the structural characterizations of the catalyst are shown in Fig. 2f and g). Computational studies (Fig. 2h) revealed that C–N bond was formed between the surface adsorbed $*CO_2$ and $*NO_2$ species and the energy barrier for forming $*CO_2NO_2$ (0.35 eV) was lower than the protonation of $*NO_2$ to $*HNO_2$ (0.62 eV), thus favoring the C–N coupling reaction over further NO_xRR. Although $*NO_2$ is not as nucleophilic as the more reduced form of N species (e.g., $*NH_2OH$, $*NH_2$), the formation of C–N bond at an early stage of $*NO_2$ can prevent the by-product generation of NO_xRR and CO_2RR, and therefore enhance the selectivities towards urea, highlighting that nucleophilicity is not the only consideration when designing an in situ generated NO_xRR intermediate for C–N coupling.

A summary of key works in building C–N bond by electrochemical NO_xRR is shown in Table 1 as below, which highlights the electrocatalyst, C and N sources, C–N coupling product, reaction conditions and electrochemical performance. Reports that utilize N_2 as the nitrogen source[46–49] are not listed in the table, as those reactions do not involve NO_xRR processes. Next, we will focus on the most recent research that couple NO_xRR with organic compounds (section 2.2) and CO_2RR (or CO_2-derived molecules such as CO and formate; section 2.3).

2.2. Couple electrochemical NO_xRR with organic compounds: utilizing $*NH_2OH$ as the nucleophile

The strong nucleophilicity of the $*NH_2OH$ intermediate generated in NO_xRR offers an ideal platform to undergo the C–N coupling process with a ketone/aldehyde to make an oxime. One of the most important oxime compounds is cyclohexanone oxime, as it can undergo Beckmann rearrangement to make caprolactam, the monomer for Nylon-6.[68] The NH_2OH required for cyclohexanone oxime production is typically generated via chemical hydrogenation of NO_x on palladium cata-
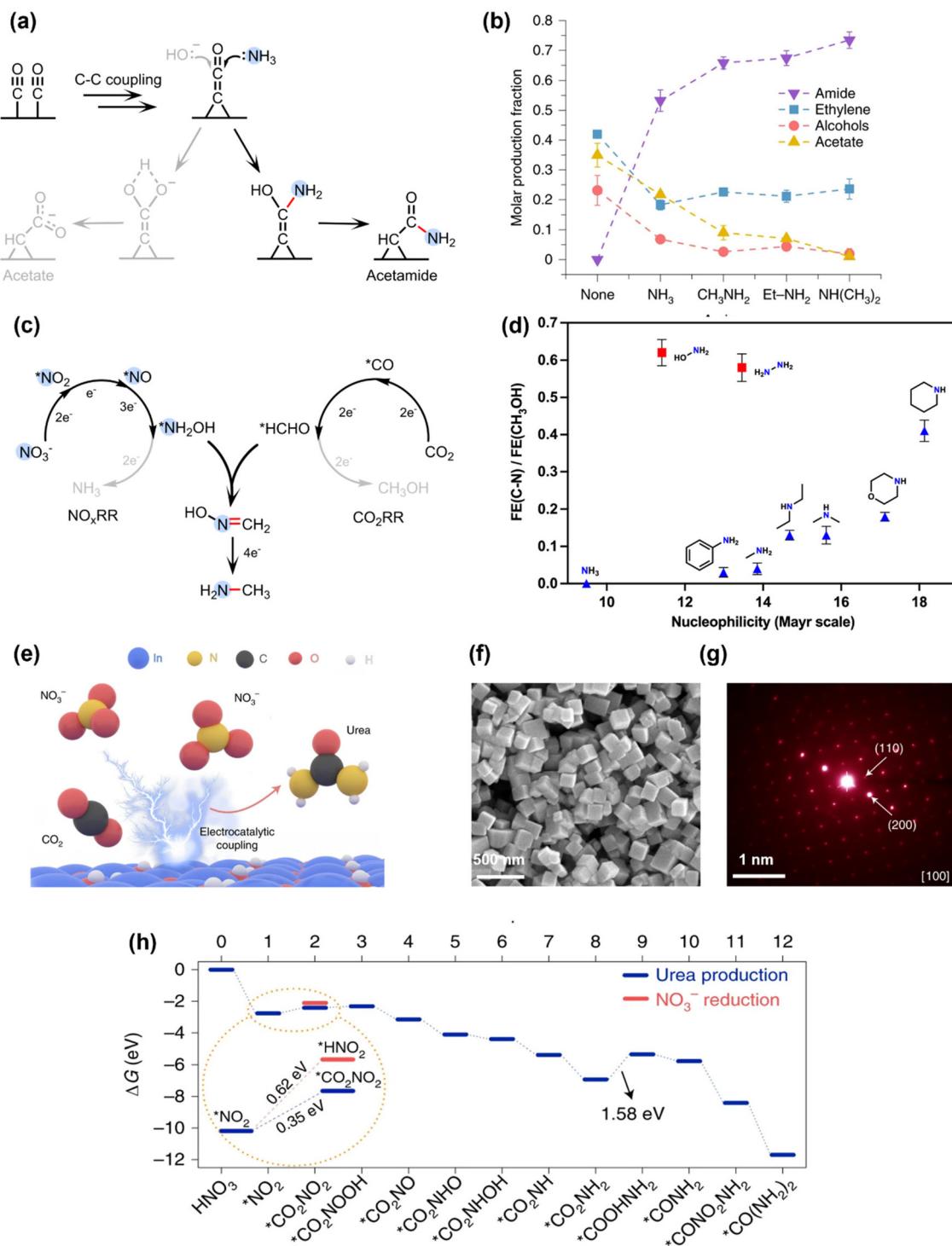
Fig. 2 Initial studies on electrochemical C−N coupling. (a) and (b) Formation of amides by adding NH_3 or amines into the electrochemical CO reduction systems.[39] Copyright 2019, Springer Nature. (c) Electrochemical co-reduction of NO_3^- and CO_2 to form methylamine *via* the coupling of $*NH_2OH$ and $*HCHO$ intermediates.[41] Copyright 2021, Springer Nature. (d) Electrochemical C−N bond formation by coupling CO_2RR with different N nucleophiles.[42] Copyright 2021, American Chemical Society. (e) Electrochemical co-reduction of NO_3^- and CO_2 to produce urea on an $In(OH)_3$ catalyst. (f) and (g) Structural characterizations of the $In(OH)_3$ catalyst by SEM and SAED. (h) Theoretical calculations for the free energy changes during the reaction, where the key C−N coupling step is thermodynamically more favorable than NO_3^- reduction.[43] Copyright 2021, Springer Nature.
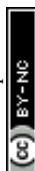
Table 1 Summary of electrochemical C–N coupling systems

Catalyst	C source	N source	Additional electrolyte	Product	Yield	FE	Potential	Partial current density	Cell configuration	Ref.
Cu	CO	NH_3	1 M KOH	Acetamide	—	38%	$-0.68 V_{RHE}$	114 mA cm^{-2}	Flow cell (3-electrode)	39
CoPc–NH$_2$	CO_2	KNO_3 (0.5 M)	0.1 M $KHCO_3$	Methylamine	—	13%	$-0.92 V_{RHE}$	3.3 mA cm^{-2}	H-cell (3-electrode)	41
In(OH)$_3$	CO_2	KNO_3 (0.1 M)	0.1 M KNO_3	Urea	—	53%	$-0.6 V_{RHE}$	0.3 mA cm^{-2}	H-cell (3-electrode)	43
Cu–S	Cyclohexanone (0.01 M)	$NaNO_2$ (0.1 M)	0.5 M phosphate buffer (pH 5.8)	Cyclohexanone oxime	92%	26%	$-0.35 V_{RHE}$	26 mA cm^{-2}	H-cell (3-electrode)	50
Fe	Cyclohexanone (0.1 M)	KNO_3 (1 M)	0.5 M K_2CO_3	Cyclohexanone oxime	100% / 100%	20% / 20%	$-0.3 V_{RHE}$ / 2.34 V (cell)	— / 100 mA cm^{-2}	H-cell (3-electrode) / Flow cell (2-electrode)	51
Zn–Cu	Cyclohexanone (0.025 M)	KNO_3 (0.1 M)	0.5 M phosphate buffer (pH 7)	Cyclohexanone oxime	97%	27%	$-0.82 V_{RHE}$	27 mA cm^{-2}	H-cell (3-electrode)	52
Al-based MOFs	Pyridine aldehyde (5 mM)	NO	0.1 M KOH	Pyridine oxime	92%	50%	$\sim-0.1 V_{RHE}$	1.6 mA cm^{-2}	H-cell (3-electrode)	53
Pd–Cu	Pyruvic acid (0.05 M)	KNO_3 (1 M)	0.2 M KH_2PO_4 + 1 M KOH (pH 5)	Alanine	55% / —	$\sim$50% / $\sim$30%	$-0.3 V_{RHE}$ / 1.7 V (cell)	$\sim$10 mA cm^{-2} / $\sim$100 mA cm^{-2}	H-cell (3-electrode) / Flow cell (2-electrode)	54
Ag	Pyruvic acid (unspecified concentration)	NO	0.1 M NaOH + 0.9 M $NaClO_4$ (with H_2SO_4 for reactor 2)	Alanine	90%	70%	$\sim$3 V (cell)	100 mA cm^{-2}	Two separate flow cells	55
Co–Fe	α-Ketoisocaproic acid (0.04 M)	NO	0.1 M HCl	Leucine	57%	32%	$-0.7 V_{RHE}$	5.4 mA cm^{-2}	H-cell (3-electrode)	56
Cu	CO_2	KNO_3 (0.1 M)	1 M KOH	Urea	—	52%	$-0.41 V_{RHE}$	115 mA cm^{-2}	Flow cell (3-electrode)	57
Zn–Cu	CO_2	KNO_3 (1000 ppm)	0.1 M $KHCO_3$	Urea	—	75%	$-0.8 V_{RHE}$	$\sim$7 mA cm^{-2}	Flow cell (3-electrode)	58
Pd$_4$Cu$_1$	CO_2	KNO_3 (0.1 M)	0.1 M $KHCO_3$	Urea	—	66%	$-0.6 V_{RHE}$	$\sim$5 mA cm^{-2}	Flow cell (3-electrode)	59
Cu–Hg	Oxalic acid (0.25 M)	KNO_3 (0.25 M)	15 wt% H_2SO_4	Glycine	46%	43%	$-1.2 V_{RHE}$	39 mA cm^{-2}	H-cell (3-electrode)	60
Cu	Formic acid (0.2 M)	$NaNO_2$ (0.02 M)	0.5 M NaOH	Formamide	90%	30%	$-0.6 V_{RHE}$	$\sim$3 mA cm^{-2}	H-cell (3-electrode)	61
Ru–Cu	CO	KNO_2 (1 M)	1 M KOH	Formamide	—	46%	$-0.5 V_{RHE}$	$\sim$5 mA cm^{-2}	H-cell (3-electrode)	62
Te–Pd	CO_2	KNO_2 (0.01 M)	0.1 M $KHCO_3$	Urea	—	12%	$-1.1 V_{RHE}$	0.8 mA cm^{-2}	H-cell (3-electrode)	63
ZnO	CO_2	$NaNO_2$ (0.1 M)	0.2 M $NaHCO_3$	Urea	—	23%	$-0.79 V_{RHE}$	5.3 mA cm^{-2}	H-cell (3-electrode)	64
TiO$_2$-Nafion	CO_2	KNO_3 (0.1 M)	—	Urea	—	40%	$-0.5 V_{RHE}$	0.8 mA cm^{-2}	H-cell (3-electrode)	65
Cu–TiO$_2$	CO_2	KNO_2 (0.02 M)	0.2 M $KHCO_3$	Urea	—	43%	$-0.4 V_{RHE}$	3.2 mA cm^{-2}	H-cell (3-electrode)	66
Cu	CO_2	KNO_3 (0.1 M)	—	Ethylamine	—	0.3%	$-1.0 V_{RHE}$	0.3 mA cm^{-2}	H-cell (3-electrode)	67

lysts[69] or oxidation of ammonia (NH_3) by O_2/H_2O_2.[68,70,71] However, these chemical processes generally require harsh reaction conditions (*e.g.*, high temperatures and/or pressures, strong acidic/alkaline solutions) and are also challenged by the safety concerns for the downstream transportation and storage of NH_2OH.[36] In contrast, electrochemical NO_xRR provides an attractive alternative strategy to generate NH_2OH *in situ* as needed to produce cyclohexanone oxime (Fig. 3a).

Recently, Zhang and coworkers demonstrated the electrosynthesis of cyclohexanone oxime by reduction of aqueous NO_2^- on a Cu–S electrocatalyst.[50] The *NH_2OH intermediate made in electrochemical NO_xRR can undergo a subsequent chemical reaction with cyclohexanone to produce oxime with a FE of 26% at 100 mA cm^{-2} and >90% yield (carbon selectivity). The Cu–S electrocatalyst was prepared by a sulfuration–electroreduction method that was previously developed by the same group.[72] A techno-economic analysis (TEA) was also performed and confirmed that the electrosynthesis strategy is profitable. Reaction intermediates were confirmed by *in situ* attenuated total reflection infrared (ATR-IR) spectroscopy, including *NO, *NH_2OH, *NH_2, and *C=N, demonstrating the key roles of the surface-adsorbed intermediates. Moreover, this electrosynthesis strategy can also be extended to a variety of ketones and aldehydes and produce the corresponding oximes with high yields and carbon selectivities (Fig. 3c). It is notable that the aromatic substrates that are usually quite active for electrochemical hydrogenation into alcohols (*e.g.* furfural, benzaldehyde) can still bear >90% selectivities towards oximes, which can potentially be explained by the low loading of the organic substrate (0.01 M ketone/aldehyde). This work demonstrates a promising strategy to make oximes with NO_2^- as the N source. Li's group has also reported a similar method to synthesize a wide range of pyridine oximes *via* the *NH_2OH intermediate generated in NO_xRR.[73]

In the meantime, the groups of Zou and Wang have also developed an electrosynthesis method for cyclohexanone oxime by utilizing the *in situ* generated *NH_2OH in NO_xRR.[51] Compared to Zhang's work, they used a 10-times higher concentration of cyclohexanone (0.1 M) and therefore the side reaction of cyclohexanone reduction into cyclohexanol must be considered. By comparing two catalyst materials (Fe and Pd, which were prepared *via* an electrical explosion method and an ethylene glycol reduction approach, respectively), they demonstrated that a good electrocatalyst for this conversion should have: (1) a strong adsorption of cyclohexanone, so that the surface-enriched cyclohexanone and *NH_2OH intermediate can form C–N bonds on the catalyst surface; and (2) a poor reduction activity for cyclohexanone to avoid the formation of the cyclohexanol byproduct. The cyclic voltammetry (CV, Fig. 3c) showed that after adding cyclohexanone into the electrolyte (without NO_x species), the Pd electrode exhibited a higher current which indicates a strong electrochemical activity for cyclohexanone reduction reaction (CHR), while the Fe electrode showed a lower current which suggests suppressed CHR activity. Theoretical calculations for the CHR processes on Fe and Pd (Fig. 3d) revealed that the adsorptions of

cyclohexanone on Fe surface and Pd surface are both thermodynamically favorable, while the first hydrogenation step is endergonic (and potentially the rate determining step) for both metals. The Gibbs energy change for this hydrogenation step on Fe (+0.59 eV) is much higher than Pd (+0.20 eV), indicating that Fe has a weaker activity for cyclohexanone reduction compared to Pd. The computation results are also consistent the CV data, as Fe has a strong surface adsorption of cyclohexanone but the subsequent hydrogenation of cyclohexanone is difficult, and therefore the surface-adsorbed cyclohexanone would 'poison' the Fe catalyst for hydrogen evolution reaction (HER) and decrease the electrochemical current. Meanwhile, the surface-enriched cyclohexanone on Fe can facilitate the nucleophilic reaction with the *NH_2OH generated in NO_xRR, and therefore Fe exhibited a ~100% carbon selectivity towards cyclohexanone oxime, whereas Pd mainly form cyclohexanol, the hydrogenation product (Fig. 3e).

Zou and Wang's work highlighted the importance of controlling the surface coverage, particularly, the adsorption of the organic substrate, in electrochemical C–N bond formation. Recently, our group also reported an electrochemical method to produce cyclohexanone oxime *via* NO_xRR and investigated the surface adsorption of NO_xRR intermediates.[52] We prepared a series of Zn/Cu alloys *via* electrodeposition and conducted a systematic study on the product selectivities on different Zn/Cu catalysts (Fig. 3f). As the Cu content increased, the NO_3RR could be driven at lower potentials and the FE for NH_3 was significantly enhanced, but the FEs for cyclohexanone oxime was quite low (<1%). The highest FE for the oxime product was achieved on $Zn_{93}Cu_7$ (FE = 27% at 100 mA cm^{-2} and $-0.82 V_{RHE}$). These observations can be explained by the trend that the weak surface adsorption of NO_xRR intermediates on pure Zn can lead to high potentials required for electroreduction, whereas strong adsorption on a Cu-rich catalyst[18] can promote this process at lower potentials but results in further reduction of *NH_2OH to NH_3 instead of forming oxime. The surface-adsorbed species was analyzed by *in situ* Raman spectroscopy (Fig. 3g), where pure Zn only showed a Raman peak at 1045 cm^{-1} for the NO_3^- in solution,[19,74] while $Zn_{93}Cu_7$ exhibited a small peak at 865 cm^{-1} that can be attributed to the surface-adsorbed *NH_2OH intermediate,[19,75] providing direct experimental evidence for this surface-adsorbed species. The pure Cu electrocatalyst exhibited two peaks at 1005 cm^{-1} and 1385 cm^{-1} corresponding to adsorbed *NO_3^- species,[19,74] indicating that Cu provides a stronger binding for NO_3^- compared to Zn, which is beneficial for electrochemical NO_3RR. Theoretical calculations (Fig. 3h) revealed that pure Cu has a lower kinetic barrier for the electroreduction of *NH_2OH to *NH_2 compared to pure Zn and $Zn_{93}Cu_7$, and thus favours the further electroreduction of *NH_2OH to NH_3 (rather than the nucleophilic reaction with ketone to make oxime). Computational results also showed that pure Zn is disadvantaged by the competing NO_3RR pathway towards N_2 (rather than NH_2OH or NH_3), which is consistent with the experimental observation that a substantial amount of N_2 was produced on Zn (FE ~ 33%). These works collectively demon-
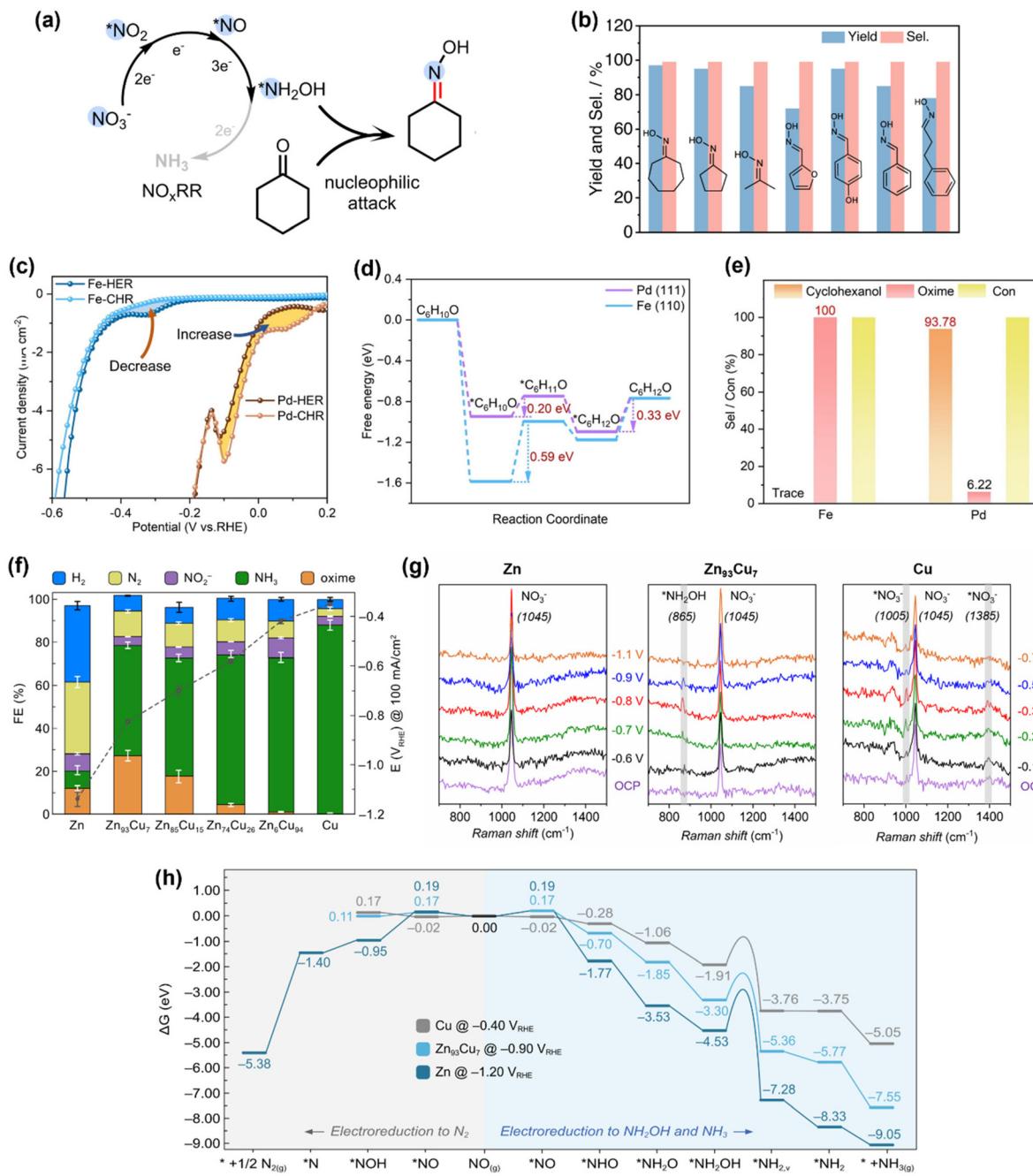
Fig. 3 Electrosynthesis of cyclohexanone oxime *via* the $*NH_2OH$ intermediate generated in NO_xRR. (a) Schematic illustration for the electrosynthesis process. (b) Reaction scope for the synthesis of oximes compounds by electrochemical NO_xRR.[50] Copyright 2023, Springer Nature. (c)–(e) Avoiding the production of cyclohexanol in electrosynthesis of cyclohexanone oxime, including the cyclic voltammetry (c) for cyclohexanone hydrogenation reaction (CHR), energy diagram (d) for CHR process, and selectivities towards cyclohexanol and oxime (e) on Fe and Pd electrocatalysts.[51] Copyright 2023, Wiley-VCH GmbH. (f)–(h) Synthesis of cyclohexanone oxime *via* electrochemical NO_xRR on a series of Zn–Cu alloy catalysts, including the electrochemical performance of different Zn/Cu catalysts (f), *in situ* Raman for Zn, $Zn_{93}Cu_7$ and Cu (g), and theoretical calculations (h) to explain the product selectivities on different Zn/Cu catalysts.[52] Copyright 2023.

strated that the surface adsorption of both organic substrate and NO_xRR intermediates plays a central role in the C–N coupling process.

Following the findings that the $*NH_2OH$ generated in NO_xRR can be used to produce oxime and the Pd electrocatalyst favors the organic hydrogenation (instead of C–N coupling), Zou and Wang groups next utilized this technique to drive the electrosynthesis of alanine (Ala), an important amino acid, from pyruvic acid (PA) and NO_3^-.[54] The $*NH_2OH$ generated in NO_xRR can undergo nucleophilic attack to the ketone group in PA to form pyruvate oxime (PO), which needs to be electrochemically hydrogenated to produce Ala (Fig. 4a).
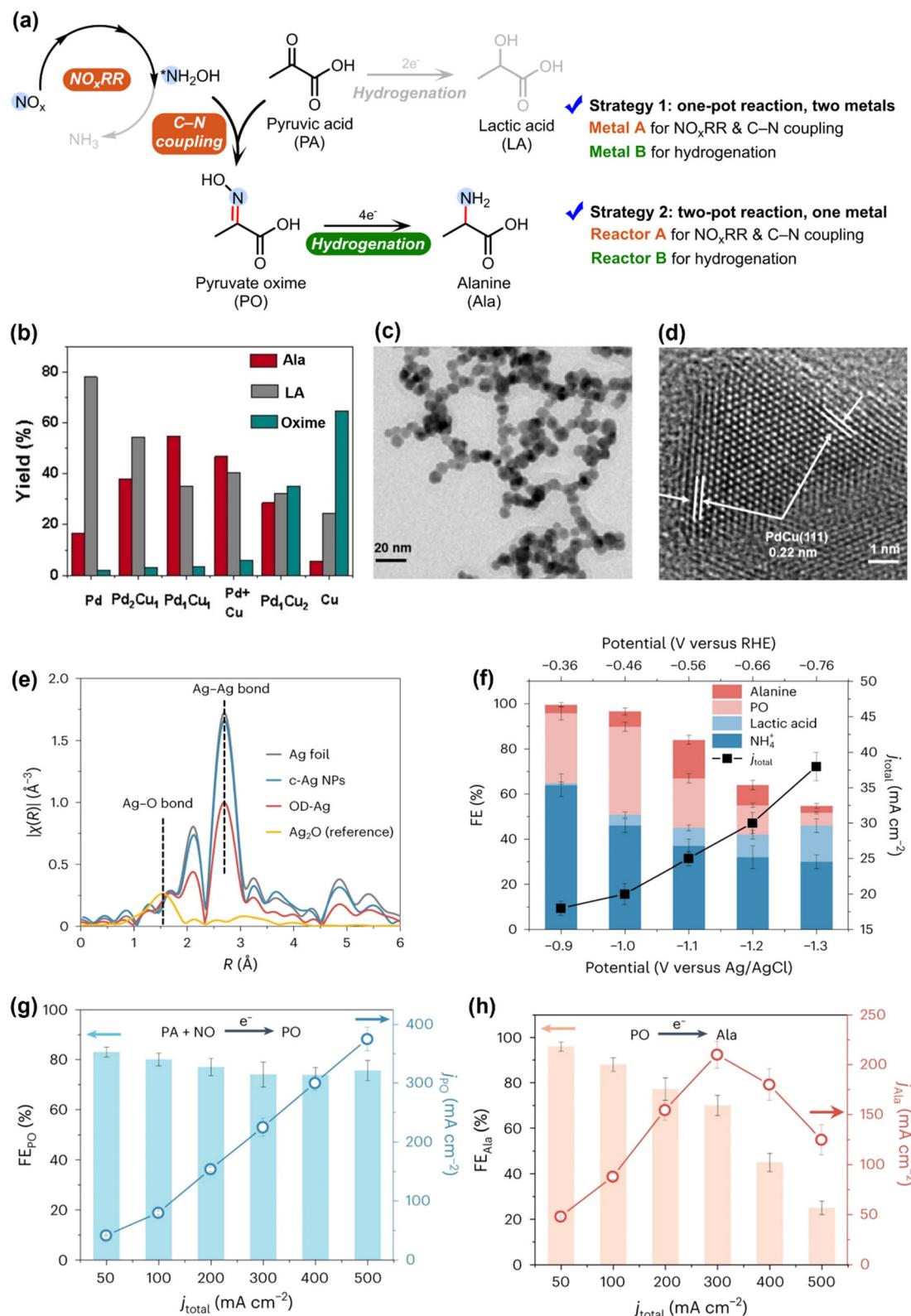
Fig. 4 Electrosynthesis of alanine *via* NO$_x$RR. (a) Reaction pathway for making analine and possible byproducts. Two strategies can be used to improve the selectivity towards analine. (b) Strategy 1, where two metals (Cu and Pd) are used to the two steps of the reaction in a one-pot system. (c) and (d) SEM and TEM images for the Pd$_1$Cu$_1$ alloy catalyst.[54] Copyright 2023, Wiley-VCH GmbH. (e)–(h) Strategy 2, where two separate reactors are used to drive the two steps of the reaction with the same OD–Ag catalyst. (e) EXAFS spectra of the OD–Ag catalyst and other Ag materials. (f) Electrochemical performance when the OD–Ag catalyst was used to drive the reaction in one-pot. (g) and (h) Electrochemical performance when the OD–Ag catalyst was used to drive the reaction in two separate reactors.[55] Copyright 2023, Springer Nature.

In order to suppress the competing reactions, including further reduction of $*NH_2OH$ to NH_3 and hydrogenation of PA to lactic acid (LA), they developed a Cu–Pd alloy catalyst and drive the one-pot synthesis of Ala (noted as strategy 1). Pure Cu (metal A) can drive the NO_xRR and C–N bond formation process to produce PO, but the hydrogenation of PO into Ala is sluggish on pure Cu (Fig. 4b). On the other side, pure Pd (metal B) is more active for hydrogenation reactions and therefore mainly produces LA from PA. To combine the advantages of the two metals, they prepared a Pd–Cu nanobead wires alloy catalyst via a solvothermal method (SEM and TEM images shown in Fig. 4c and d), where a maximum yield at 55% for Ala can be achieved on the Pd_1Cu_1 alloy catalyst (Fig. 4b). In a similar way, Li and co-workers also demonstrated the electrosynthesis of 13 different amino acids through NO_xRR on a Co–Fe alloy electrocatalyst.[56]

Another strategy to overcome the challenges in making Ala is to spatially decouple the synthesis of PO and the subsequent hydrogenation of PO to Ala, and drive the reaction in a two-pot process. Zhang et al. recently developed an electrosynthesis method to produce Ala from PA and NO with two separate reactors (denoted as strategy 2, Fig. 4e–g), where NO_xRR and C–N coupling occur in reactor A, and the PO produced in reactor A is further converted to Ala in reactor B.[55] They pre-pared an oxide-derived Ag (OD–Ag) catalyst via in situ electrore-duction to drive both steps. As the shown in the EXAFS spectra (Fig. 4e), the Ag–O bond has been removed in OD–Ag, indicating the full conversion from Ag_2O to OD–Ag catalyst, and the smaller Ag–Ag bond in OD–Ag compared to Ag foil also revealed the low-coordination sites, which are also important in the electrocatalysis process. When the OD–Ag catalyst was used to drive the one-pot synthesis of Ala (Fig. 4f), the FE for Ala was quite low (<20%) and a series of byproducts (e.g., NH_4^+, LA) were formed due the rapid PO formation but the slow PO hydrogenation steps. In contrast, when the OD–Ag catalyst was used in two separate reactors (Fig. 4g and h), both the PO formation (PA + NO → PO, reactor A) and the PO hydro-genation (PO → Ala, reactor B) can be driven with high FEs. The aforementioned works collectively demonstrated the importance of designing complementary bi-metal (strategy 1) or bi-reactor (strategy 2) systems to match the different requirements in PO formation and PO hydrogenation.

2.3. Couple electrochemical NO_xRR and CO_2RR

Based on the similarities between electrochemical CO_2RR and NO_xRR, such as surface adsorption, electron transfer and cata-lyst design, a series of bi-functional catalysts have been devel-
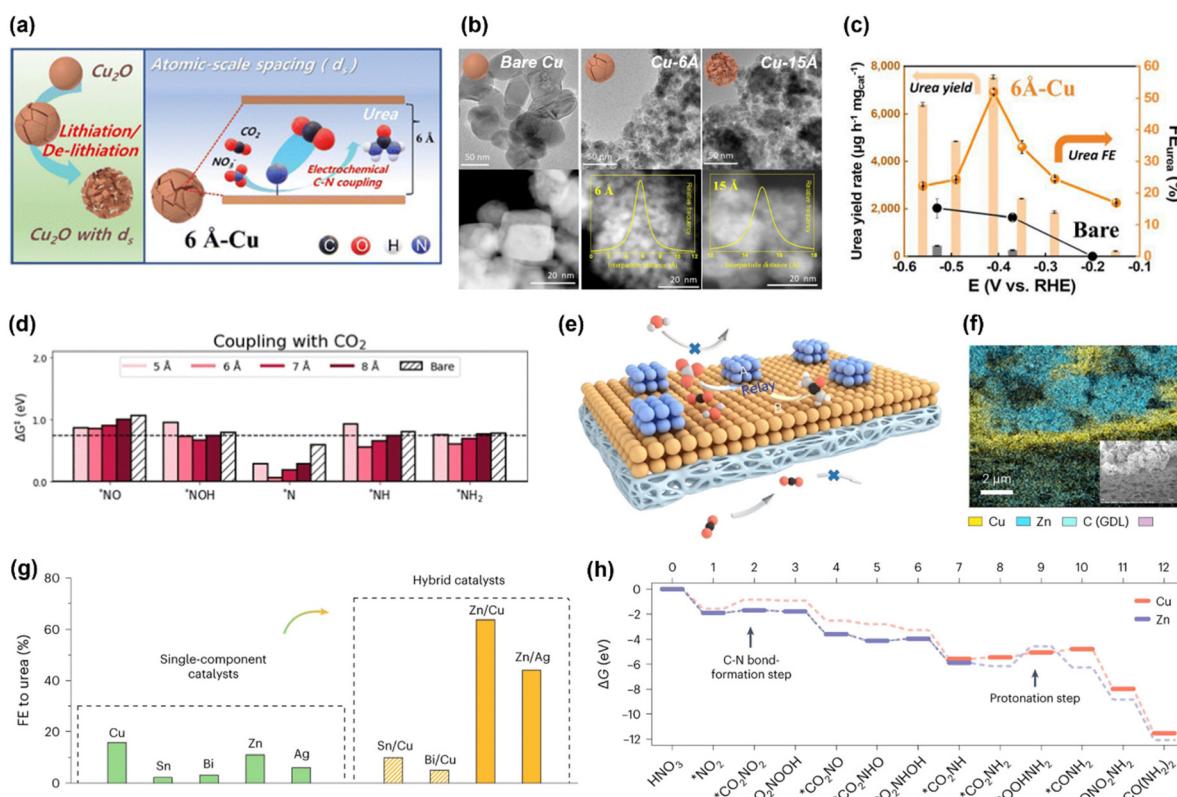

Fig. 5 Electrochemical co-reduction of CO_2 and NO_3^- into urea. (a) Schematic illustration of the Cu electrocatalyst with atomic scale spacings. (b) TEM and STEM images of the bare Cu, Cu with 6 Å spacing and Cu with 15 Å spacing. (c) Electrochemical performance for urea production on the 6 Å-Cu and bare Cu. (d) Kinetic barriers for the C–N coupling for CO_2 with possible NO_xRR intermediates.[57] Copyright 2023, Royal Society of Chemistry. (e) Schematic illustration of the Zn–Cu alloy catalyst for urea production. (f) Elemental mapping of Zn and Cu in the alloy catalyst. (g) FE for urea on different metals and alloys. (h) Theoretical calculations for the free energy changes during the reaction.[58] Copyright 2023, Springer Nature.

oped to enable the co-reduction of CO_2 and NO_x into small organonitrogen molecules. For example, urea is the most widely studied co-reduction product due to its large market demands as a fertilizer. Following the study by Yu's lab in 2021, where urea is produced with a FE as high as 53% but a relatively low current density at 0.6 mA cm^{-2} (as described in 2.1),[43] researchers have recently significantly improved the FE and current density for the co-reduction of CO_2 and NO_3^- into urea. In 2023, Kwon and coworkers prepared a Cu electrocatalyst with atomic scale spacings (d_s) between two facets of Cu, which can facilitate the production of urea (Fig. 5a).[57] The atomic-scale spacings were created by an electrochemical lithiation process on the Cu nanoparticles and the size of spacings was controlled by degree of lithiation, as revealed by TEM and STEM in Fig. 5b. The Cu with a d_s of 6 Å can achieves a FE for urea of 52% at 220 mA cm^{-2} and $-0.41V_{RHE}$, which are significantly higher than the bare Cu without lithiation treatment (Fig. 5c). Computational studies revealed that atomic-scale spacings can efficiently lower the kinetic barriers for C–N coupling (Fig. 5d): the kinetic barriers for CO_2 coupling with a variety of possible NO_xRR intermediates (*NO, *NOH, *N, *NH, *NH$_2$) are all decreased in the Cu with 6 Å spacing. Recently, Ye's lab has also reported that an atomically-dispersed Cu in Pd catalyst (Pd$_4$Cu$_1$) can convert CO_2 and NO_3^- into urea with a FE of 66% and 436.9 mmol g$_{cat.}^{-1}$ h^{-1} at $-0.6V_{RHE}$, as well as a long cycling stability of 1000 h.[59] These works highlighted the importance of controlling the morphology of the electrocatalyst at atomic scale in facilitating the electrochemical urea production.

Similar to the electrosynthesis of Ala, another strategy to enhance the electrochemical co-reduction of CO_2 and NO_3^- into urea is making a bimetallic alloy catalyst, where one metal can facilitate the key C–N coupling step, and the other metal can facilitate the electron and proton transfer steps (co-reduction of CO_2 and NO_3^- into urea is a 16-electron process). Recently, Sargent's lab developed a Zn–Cu hybrid catalyst for electrosynthesis of urea, where Zn can facilitate the C–N coupling step and Cu can reduce the energy required for a key protonation step in making urea (Fig. 5e and f).[58] The Zn–Cu hybrid catalyst was prepared by spray-coating an incomplete layer of Zn on top of the Cu layer (Zn and Cu were both commercially available nanoparticles). Compared to single metal catalysts, bimetallic alloy catalysts such as Zn–Cu and Zn–Ag can significantly improve the FE for urea (Fig. 5g). Theoretical calculations indicated that the C–N bond formation (CO_2 + *NO$_2$ → *CO$_2$NO$_2$) is more favorable on the surface of Zn compared to Cu, whereas the endergonic step for the protonation of *CO$_2$NH$_2$ to *COOHNH$_2$ (potentially the rate determining step) requires less energy on Cu compared to Zn (Fig. 5h). With this relay catalyst design, CO_2 gas and simulated wastewater containing 1000 ppm NO_3^- can be converted to urea with a FE of 75% and a total current density of 10 mA cm^{-2} at $-0.8V_{RHE}$, which can last for 32 hours.

In addition to urea, other small organonitrogen molecules can also be produced *via* the coupling CO_2RR and NO_xRR, such as methylamine[41] as described in 2.1. Researchers have also proved that NO_xRR intermediates can undergo nucleophilic attack to CO_2-derived molecules. For example, Nam and co-
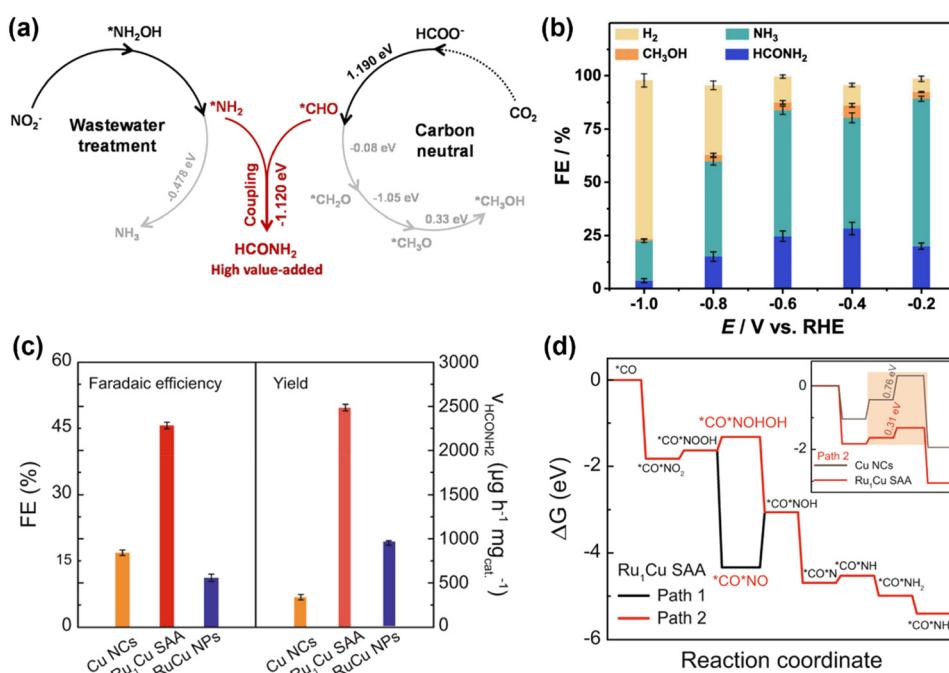
Fig. 6 Electrosynthesis of formamide from NO_2^- and CO_2-derived molecules. (a) and (b) Electrochemical co-reduction of NO_2^- and formic acid into formamide.[61] Copyright 2023, American Chemical Society. (c) and (d) Electrochemical co-reduction of NO_2^- and CO into formamide.[62] Copyright 2023, Springer Nature.

workers reported in 2021 that oxalic acid, a CO_2RR product, can be converted to glycine *via* electrochemical NO_3^- reduction.[60] Recently, Zhang's lab demonstrated that the electrochemical co-reduction of NO_2^- and the CO_2-derived formic acid can yield formamide on a Cu catalyst (Fig. 6a), which was prepared by electroreduction of Cu_2O nanocubes.[61] At $-0.6V_{RHE}$, NO_2^- and formic acid can be converted to formamide with a FE ~ 30% (Fig. 6b). Mechanistic studies suggested that the C–N coupling step occurs between the $*NH_2$ and $*CHO$ intermediates ($\Delta G = -1.12$ eV), which is thermodynamically favored compared to thermoneutral step of further reduction of $*CHO$ ($\Delta G = -0.08$ eV), whereas the further reduction of $*NH_2$ is also thermodynamically feasible ($\Delta G = -0.48$ eV). These calculations results are consistent with the experimental observations that NH_3 (*i.e.*, over-reduction of NO_2^-) was the main by-product, while the generation of CH_3OH (*i.e.*, over-reduction of CO_2) is minimal.

Tan and Coworkers also reported an electrochemical method to convert NO_2^- and CO into formamide on a single-atom alloy (SAA) electrocatalyst with atomically dispersed Ru atoms on Cu nanoclusters.[62] The Ru–Cu SAA catalysts were prepared by thermal reduction of Cu^{2+} to make Cu nanoclusters and then introducing Ru single atom onto the surface of Cu nanoclusters through galvanic replacement reaction. Formamide can be produced with a FE of 46% at $-0.5V_{RHE}$, which is significantly higher than pure Cu or Ru–Cu nanoparticles (Fig. 6c), thus highlighting the importance of bimetallic alloy as well as single-atom catalyst. Computational studies (Fig. 6d) showed that Ru can lower the energy barriers for the hydrogenation steps of the $*CO*NO_2$ intermediate ($*CO*NO_2 \rightarrow *CO*NOOH \rightarrow *CO*NOHOH$), and thus can facilitate the formamide production compared to pure Cu.

3. Summary and outlook

The aforementioned works provide attractive methods to build C–N bonds *via* electrochemical NO_xRR. In particular, some key strategies and considerations are highlighted to enhance the selectivities towards the desired C–N coupling products, as summarized as below:

(1) Choosing a suitable nucleophile for C–N coupling. The NO_xRR intermediates, such as $*NH_2OH$ and $*NH_2$, are usually more nucleophilic than both the reactants (*e.g.*, NO_3^-, NO_2^-) and the final product of NO_xRR (NH_3) and therefore can facilitate the C–N coupling step. On the other side, utilizing a NO_xRR intermediate at the early stage (*e.g.*, $*NO_2$) as the nucleophile for C–N coupling can prevent the formation of byproducts (*e.g.*, N_2, NH_3).

(2) Controlling the surface adsorptions of both nucleophile (*i.e.*, NO_xRR intermediates) and electrophile (*i.e.*, CO_2RR intermediates or organic substrate). The electrocatalyst should have sufficient adsorptions of the reactants and intermediates so that the electroreduction can proceed at low potentials, but the adsorptions should not be too strong so that the product can desorb from the catalyst and avoid over-reduction.

(3) Designing bimetallic alloy catalysts or bi-reactor system to drive the C–N coupling step and hydrogenation step separately. The C–N coupling step and electroreduction step can have quite different requirement for reaction conditions, such as catalyst, potential, pH, *etc.*, and therefore it would be helpful to decouple the two steps by designing an alloy catalyst containing two metals or a tandem system with two separate reactors.

(4) Preparing electrocatalysts with nano-/atomic-scale surface structures, single-atom structures, single crystal facets, or alloy compositions. The catalysts with nano-/atomic-scale morphologies or single-atom structures can usually enhance the reaction rate by lowering the energy barriers and a specific single crystal facet can potentially improve the selectivity towards a certain product. Making alloy electrocatalysts can also tune the surface adsorptions of intermediates, meet different requirements for C–N coupling step and electroreduction step, and allow synergetic effects to improve the FE.

Despite these distinctive methods, there are still some challenges and problems in this area as listed below:

(1) The formation of the desired C–N coupling product is in competition of other reactions. For example, the co-reduction of NO_x and CO_2 can obviously generate a series of byproducts without C–N coupling, such as NH_3, N_2, CO, formate, *etc.* The HER can also be a significant competing reaction. When organic compounds (*e.g.* cyclohexanone) are present in the electrolyte, the organic hydrogenation reaction can also lower the FE for C–N coupling. Furthermore, the C–N coupling products could also be further reduced and the desired chemical structures (*e.g.* oxime) may be lost.

(2) The reaction pathway and key intermediates for C–N coupling are still not very clear, particularly for the formation of urea. The NH_2OH-mediated C–N coupling pathways (*e.g.* in the formations of amine, oxime, amino acid) are relatively better understood and researchers can confirm that the surface-adsorbed $*NH_2OH$ is the key intermediate to build the C–N bond. However, it is still unclear that the C–N bond in urea is formed at which stage of electrochemical NO_xRR. Several possible intermediates have been proposed as key species for C–N coupling, such as $*NO_2$, $*NO$, $*N$, and $*NH_2$, but the direct experimental evidence is still rarely reported. The intermediates at the early stage of NO_xRR (*e.g.* $*NO_2$, $*NO$) can potentially avoid the generation of byproducts in NO_xRR and CO_2RR, whereas the intermediates at the later stage (*e.g.* $*N$, $*NH_2$) are more nucleophilic and therefore more energy-favorable. More in-depth mechanistic studies, ideally *in situ* spectroscopies, are needed to better understand the reaction pathway for making urea.

(3) The NO_xRR to build C–N bond is also challenged by similar factors in the pure electrochemical NO_xRR (*i.e.* without C–N coupling). For example, the electrochemical reduction of NO_3^- is usually limited by the large overpotential caused by the sluggish rate-determining step of NO_3^- reduction to NO_2^- [32] (the theoretical potential is $+0.69V_{RHE}$ whereas the operation potential is usually from $-1.0V_{RHE}$ to $0V_{RHE}$). The C–N coupling reaction is also challenged by other common

problems in pure electrochemical NO_xRR, such as catalyst poisoning caused by the excessive adsorption of $*NO_2$,[18] degradation of metallic catalysts in concentrated NH_3 solution, difficulties in utilizing diluted NO_x in real-world wastewater, *etc.*

We also look into a few possible future directions that can be pursued to improve the performance, profitability and impact of this research area:

(1) The nitrogen selectivity/utilization efficiency should be improved. Current electrochemical C–N coupling systems typically contain NO_x species with a concentration that is about one order of magnitude higher than the organic substrate to allow the full conversion of organic substrate. However, the high loading of NO_x species also decreases the FE and N utilization efficiency for the desired product. The main N-containing product is usually NH_3 (and N_2 in some cases). Considering many studies utilize the $*NH_2OH$ intermediate as the nucleophile, it is necessary to tune the surface adsorption of $*NH_2OH$ to prevent its over-reduction into NH_3 and reduce the loading NO_x required for full conversion of organic substrate. For example, Zhang's lab recently proved that the electroreduction of NO favored the formation of NH_2OH (FE up to 80%) on Co single-atom catalysts while the NO reduction on Co nanoparticles mainly generated NH_3.[76] The selectivity between NH_2OH and NH_3 was tuned by regulating the adsorption configuration of NO: the linear adsorption of NO on the single-atom catalysts can maintain the N–O bond and allow the NO reduction to stop at the stage of NH_2OH, while the bridge adsorption of NO on the nanoparticles would weaken the N–O bond to produce NH_3. It is also notable that the NO_xRR may not proceed through the $*NH_2OH$-mediated pathway (*i.e.*, $NO_x \rightarrow *NH_2OH \rightarrow *NH_2 \rightarrow NH_3$); instead, it could also undergo the $*N$-mediated pathway: $NO_x \rightarrow *N$, and then the surface-adsorbed $*N$ can either make N_2 ($2 *N \rightarrow N_2$), or produce NH_3 ($*N \rightarrow *NH \rightarrow *NH_2 \rightarrow NH_3$).[9,37] In either case, $*NH_2OH$ will not be produced. Therefore, the reaction mechanism that involves surface-adsorbed intermediates should be further understood (as discussed below) to prevent the $*N$-mediated pathway and enhance formation of $*NH_2OH$. In addition, pulsed electrolysis methods, which are known to tune the local concentration of NO_x species near the electrode and optimize the surface adsorption configuration of intermediates in electrochemical NO_xRR to NH_3,[77–79] could also be used to improve the N selectivity in C–N coupling.

(2) Mechanistic study by detecting the reaction intermediates with *in situ* technologies. The surface-adsorbed reaction intermediates play a central role in electrochemical NO_xRR and C–N coupling, such as $*NO$, $*NOH$, $*N$, $*NH_2OH$ and $*NH_2$. Those intermediates can be studied by *in situ* spectroscopies, such as ATR-IR and Raman.[43,50] The hydrogen radicals at the electrode surface, which determine the electrochemical hydrogenation of NO_xRR intermediates, can be investigated by electron paramagnetic resonance (EPR).[14,32] The catalytic sites of electrocatalyst can be monitored by *in situ* X-ray diffraction (XRD), X-ray absorption near edge structure (XANES) and extended X-ray absorption fine structure (EXAFS) technologies.[31,32] Moreover, the gaseous products and inter-

mediates can also be analyzed by on-line differential electrochemical mass spectrometry (DEMS) during the electrochemical reaction.[14,32] More *in situ* technologies should be adapted together with computational studies to systematically understand the reaction pathways towards different N-containing products (N_2, NH_3, C–N coupling products, *etc.*), and how the selectivities are controlled by catalyst structure and reaction conditions (potential, concentrations, pH, *etc.*).

(3) Electrochemical co-reduction of CO_2 and NO_x into C_{2+} organonitrogen molecules. Co-reduction of CO_2 and NO_x to form C–N bonds have provided an attractive route to produce organonitrogen compounds. Despite these distinctive methods, current studies mainly focus on producing C_1 organonitrogen compounds. A co-reduction system that can build the C–N bonds in C_{2+} organonitrogen molecules, which tend to be more valuable, has barely been reported. In CO_2RR studies, a microfluidic flow reactor has been developed:[80–84] an ion exchange membrane and an aqueous alkaline liquid layer, which is known to facilitate CO_2RR towards C_{2+} products,[81,82] are sandwiched between the anode and cathode. In a similar way, this flow reactor design could also enhance the formation of C_{2+} organonitrogen molecules in CO_2–NO_x co-reduction. The reaction can occur at the gas–liquid–solid interface, where the electrocatalyst is in contact with aqueous electrolyte (OH^- and NO_3^-/NO_2^-) and gaseous CO_2. A key challenge here that making C_{2+} organonitrogen products will require the formation of both C–C and C–N bonds, where the strategies of making bimetallic alloy catalysts could be employed to facilitate the C–C and C–N bonds formation separately.

(4) Utilize industrial/agricultural wastewater containing NO_3^-/NO_2^- to produce organonitrogen compounds. Compared to the NO_3^-/NO_2^- solutions in lab, the real-world wastewater usually has lower concentrations of NO_3^-/NO_2^-, unsuitable pH values, and complicated components such as organic residues, metal cations that can poison the catalyst through electrodeposition on the electrode,[85,86] anions that may change the product selectivity (*e.g.*, Cl^- is known to facilitate NO_xRR towards N_2),[87–89] *etc.*, these factors will affect the C–N coupling reaction. Therefore, some pre-treatment of wastewater may be needed and a more robust electrocatalyst will be required. Furthermore, the scalability, energy efficiency, economic cost, separation of the organonitrogen products, and long-term stability will also be important considerations to develop a profitable NO_xRR electrolyzer for industrial implementation.

Conflicts of interest

The authors declare no competing financial interest.

Acknowledgements

References

1 M. C. Leech and K. Lam, *Nat. Rev. Chem.*, 2022, **6**, 275–286.

2 M. C. Leech, A. D. Garcia, A. Petti, A. P. Dobbs and K. Lam, *React. Chem. Eng.*, 2020, **5**, 977–990.

3 M. Yan, Y. Kawamata and P. S. Baran, *Chem. Rev.*, 2017, **117**, 13230–13319.

4 L. F. T. Novaes, J. Liu, Y. Shen, L. Lu, J. M. Meinhardt and S. Lin, *Chem. Soc. Rev.*, 2021, **50**, 7941–8002.

5 A. Wiebe, T. Gieshoff, S. Möhle, E. Rodrigo, M. Zirbes and S. R. Waldvogel, *Angew. Chem., Int. Ed.*, 2018, **57**, 5594–5619.

6 S. Nitopi, E. Bertheussen, S. B. Scott, X. Liu, A. K. Engstfeld, S. Horch, B. Seger, I. E. L. Stephens, K. Chan, C. Hahn, J. K. Nørskov, T. F. Jaramillo and I. Chorkendorff, *Chem. Rev.*, 2019, **119**, 7610–7672.

7 M. B. Ross, P. De Luna, Y. Li, C.-T. Dinh, D. Kim, P. Yang and E. H. Sargent, *Nat. Catal.*, 2019, **2**, 648–658.

8 P. De Luna, C. Hahn, D. Higgins, S. A. Jaffer, T. F. Jaramillo and E. H. Sargent, *Science*, 2019, **364**, 350.

9 H. Xu, Y. Ma, J. Chen, W.-X. Zhang and J. Yang, *Chem. Soc. Rev.*, 2022, **51**, 2710–2758.

10 P. H. van Langevelde, I. Katsounaros and M. T. M. Koper, *Joule*, 2021, **5**, 290–294.

11 W. Chen, X. Yang, Z. Chen, Z. Ou, J. Hu, Y. Xu, Y. Li, X. Ren, S. Ye, J. Qiu, J. Liu and Q. Zhang, *Adv. Funct. Mater.*, 2023, 2300512, DOI: 10.1002/adfm.202300512.

12 R. Cassia, M. Nocioni, N. Correa-Aragunde and L. Lamattina, *Front. Plant Sci.*, 2018, **9**, 273.

13 K. Fan, W. Xie, J. Li, Y. Sun, P. Xu, Y. Tang, Z. Li and M. Shao, *Nat. Commun.*, 2022, **13**, 7958.

14 H. Liu, X. Lang, C. Zhu, J. Timoshenko, M. Rüscher, L. Bai, N. Guijarro, H. Yin, Y. Peng, J. Li, Z. Liu, W. Wang, B. R. Cuenya and J. Luo, *Angew. Chem., Int. Ed.*, 2022, **61**, e202202556.

15 J. Li, G. Zhan, J. Yang, F. Quan, C. Mao, Y. Liu, B. Wang, F. Lei, L. Li, A. W. M. Chan, L. Xu, Y. Shi, Y. Du, W. Hao, P. K. Wong, J. Wang, S.-X. Dou, L. Zhang and J. C. Yu, *J. Am. Chem. Soc.*, 2020, **142**, 7036–7046.

16 Y. Zhang, Y. Wang, L. Han, S. Wang, T. Cui, Y. Yan, M. Xu, H. Duan, Y. Kuang and X. Sun, *Angew. Chem., Int. Ed.*, 2023, **62**, e202213711.

17 R. Zhao, Q. Yan, L. Yu, T. Yan, X. Zhu, Z. Zhao, L. Liu and J. Xi, *Adv. Mater.*, 2023, **35**, 2306633.

18 L. Wu, J. Feng, L. Zhang, S. Jia, X. Song, Q. Zhu, X. Kang, X. Xing, X. Sun and B. Han, *Angew. Chem., Int. Ed.*, 2023, e202307952, DOI: 10.1002/anie.202307952.

19 W. Gao, K. Xie, J. Xie, X. Wang, H. Zhang, S. Chen, H. Wang, Z. Li and C. Li, *Adv. Mater.*, 2023, **35**, 2202952.

20 M. Xie, S. Tang, Z. Li, M. Wang, Z. Jin, P. Li, X. Zhan, H. Zhou and G. Yu, *J. Am. Chem. Soc.*, 2023, **145**, 13957–13967.

21 J. Yang, H. Qi, A. Li, X. Liu, X. Yang, S. Zhang, Q. Zhao, Q. Jiang, Y. Su, L. Zhang, J.-F. Li, Z.-Q. Tian, W. Liu, A. Wang and T. Zhang, *J. Am. Chem. Soc.*, 2022, **144**, 12062–12071.

22 Y. Wang, A. Xu, Z. Wang, L. Huang, J. Li, F. Li, J. Wicks, M. Luo, D.-H. Nam, C.-S. Tan, Y. Ding, J. Wu, Y. Lum, C.-T. Dinh, D. Sinton, G. Zheng and E. H. Sargent, *J. Am. Chem. Soc.*, 2020, **142**, 5702–5708.

23 G.-F. Chen, Y. Yuan, H. Jiang, S.-Y. Ren, L.-X. Ding, L. Ma, T. Wu, J. Lu and H. Wang, *Nat. Energy*, 2020, **5**, 605–613.

24 X. He, Z. Li, J. Yao, K. Dong, X. Li, L. Hu, S. Sun, Z. Cai, D. Zheng, Y. Luo, B. Ying, M. S. Hamdy, L. Xie, Q. Liu and X. Sun, *iScience*, 2023, **26**, 107100.

25 J. Liang, Z. Li, L. Zhang, X. He, Y. Luo, D. Zheng, Y. Wang, T. Li, H. Yan, B. Ying, S. Sun, Q. Liu, M. S. Hamdy, B. Tang and X. Sun, *Chem*, 2023, **9**, 1768–1827.

26 L. Yue, W. Song, L. Zhang, Y. Luo, Y. Wang, T. Li, B. Ying, S. Sun, D. Zheng, Q. Liu, A. Farouk, M. S. Hamdy, S. Alfaifi and X. Sun, *Small Struct.*, 2023, **4**, 2300168.

27 X. He, X. Li, X. Fan, J. Li, D. Zhao, L. Zhang, S. Sun, Y. Luo, D. Zheng, L. Xie, A. M. Asiri, Q. Liu and X. Sun, *ACS Appl. Nano Mater.*, 2022, **5**, 14246–14250.

28 H. Wang, F. Zhang, M. Jin, D. Zhao, X. Fan, Z. Li, Y. Luo, D. Zheng, T. Li, Y. Wang, B. Ying, S. Sun, Q. Liu, X. Liu and X. Sun, *Mater. Today Phys.*, 2023, **30**, 100944.

29 X. Fan, C. Liu, Z. Li, Z. Cai, L. Ouyang, Z. Li, X. He, Y. Luo, D. Zheng, S. Sun, Y. Wang, B. Ying, Q. Liu, A. Farouk, M. S. Hamdy, F. Gong, X. Sun and Y. Zheng, *Small*, 2023, **19**, 2303424.

30 Z. Li, Q. Zhou, J. Liang, L. Zhang, X. Fan, D. Zhao, Z. Cai, J. Li, D. Zheng, X. He, Y. Luo, Y. Wang, B. Ying, H. Yan, S. Sun, J. Zhang, A. A. Alshehri, F. Gong, Y. Zheng and X. Sun, *Small*, 2023, **19**, 2300291.

31 F. Y. Chen, Z. Y. Wu, S. Gupta, D. J. Rivera, S. V. Lambeets, S. Pecaut, J. Y. T. Kim, P. Zhu, Y. Z. Finfrock, D. M. Meira, G. King, G. Gao, W. Xu, D. A. Cullen, H. Zhou, Y. Han, D. E. Perea, C. L. Muhich and H. Wang, *Nat. Nanotechnol.*, 2022, **17**, 759–767.

32 S. Han, H. Li, T. Li, F. Chen, R. Yang, Y. Yu and B. Zhang, *Nat. Catal.*, 2023, **6**, 402–414.

33 D.-X. Liu, Z. Meng, Y.-F. Zhu, X.-F. Sun, X. Deng, M.-M. Shi, Q. Hao, X. Kang, T.-Y. Dai, H.-X. Zhong, J. Yan and Q. Jiang, *Angew. Chem., Int. Ed.*, 2023, e202315238, DOI: 10.1002/anie.202315238.

34 J. Shao, H. Jing, P. Wei, X. Fu, L. Pang, Y. Song, K. Ye, M. Li, L. Jiang, J. Ma, R. Li, R. Si, Z. Peng, G. Wang and J. Xiao, *Nat. Energy*, 2023, **8**, 1273–1283.

35 L. Shi, L. Liu, B. Yang, G. Sheng and T. Xu, *Sustainability*, 2020, **12**, 3793.

36 L. O. Cisneros, W. J. Rogers and M. Sam Mannan, *Thermochim. Acta*, 2004, **414**, 177–183.

37 P. Liao, J. Kang, R. Xiang, S. Wang and G. Li, *Angew. Chem., Int. Ed.*, 2023, e202311752, DOI: 10.1002/anie.202311752.

38 J. Li, Y. Zhang, K. Kuruvinashetti and N. Kornienko, *Nat. Rev. Chem.*, 2022, **6**, 303–319.

39 M. Jouny, J.-J. Lv, T. Cheng, B. H. Ko, J.-J. Zhu, W. A. Goddard and F. Jiao, *Nat. Chem.*, 2019, **11**, 846–851.

40 J. Li and N. Kornienko, *Chem. Sci.*, 2022, **13**, 3957–3964.

41 Y. Wu, Z. Jiang, Z. Lin, Y. Liang and H. Wang, *Nat. Sustainability*, 2021, **4**, 725–730.

42 C. L. Rooney, Y. Wu, Z. Tao and H. Wang, *J. Am. Chem. Soc.*, 2021, **143**, 19983–19991.

43 C. Lv, L. Zhong, H. Liu, Z. Fang, C. Yan, M. Chen, Y. Kong, C. Lee, D. Liu, S. Li, J. Liu, L. Song, G. Chen, Q. Yan and G. Yu, *Nat. Sustainability*, 2021, **4**, 868–876.

44 Y. Wu, Z. Jiang, X. Lu, Y. Liang and H. Wang, *Nature*, 2019, **575**, 639–642.

45 J. Liu, G. Chen, Y. Yu, Y. Wu, M. Zhou, W. Zhang, H. Qin, C. Lv and W. Fu, *New J. Chem.*, 2015, **39**, 1930–1937.

46 C. Chen, X. Zhu, X. Wen, Y. Zhou, L. Zhou, H. Li, L. Tao, Q. Li, S. Du, T. Liu, D. Yan, C. Xie, Y. Zou, Y. Wang, R. Chen, J. Huo, Y. Li, J. Cheng, H. Su, X. Zhao, W. Cheng, Q. Liu, H. Lin, J. Luo, J. Chen, M. Dong, K. Cheng, C. Li and S. Wang, *Nat. Chem.*, 2020, **12**, 717–724.

47 M. Yuan, J. Chen, Y. Bai, Z. Liu, J. Zhang, T. Zhao, Q. Wang, S. Li, H. He and G. Zhang, *Angew. Chem., Int. Ed.*, 2021, **60**, 10910–10918.

48 M. Yuan, J. Chen, Y. Xu, R. Liu, T. Zhao, J. Zhang, Z. Ren, Z. Liu, C. Streb, H. He, C. Yang, S. Zhang and G. Zhang, *Energy Environ. Sci.*, 2021, **14**, 6605–6615.

49 M. Yuan, J. Chen, Y. Bai, Z. Liu, J. Zhang, T. Zhao, Q. Shi, S. Li, X. Wang and G. Zhang, *Chem. Sci.*, 2021, **12**, 6048–6058.

50 Y. Wu, J. Zhao, C. Wang, T. Li, B.-H. Zhao, Z. Song, C. Liu and B. Zhang, *Nat. Commun.*, 2023, **14**, 3057.

51 Y. Wu, W. Chen, Y. Jiang, Y. Xu, B. Zhou, L. Xu, C. Xie, M. Yang, M. Qiu, D. Wang, Q. Liu, Q. Liu, S. Wang and Y. Zou, *Angew. Chem., Int. Ed.*, 2023, e202305491, DOI: **10.1002/anie.202305491**.

52 J. Sharp, A. Ciotti, H. Andrews, S. Udayasurian, M. García-Melchor and T. Li, *ChemRxiv*, 2023, DOI: **10.26434/chemr-xiv-2023-q265h**.

53 R. Xiang, S. Wang, P. Liao, F. Xie, J. Kang, S. Li, J. Xian, L. Guo and G. Li, *Angew. Chem., Int. Ed.*, 2023, e202312239, DOI: **10.1002/anie.202312239**.

54 J. Wu, L. Xu, Z. Kong, K. Gu, Y. Lu, X. Wu, Y. Zou and S. Wang, *Angew. Chem., Int. Ed.*, 2023, e202311196, DOI: **10.1002/anie.202311196**.

55 M. Li, Y. Wu, B.-H. Zhao, C. Cheng, J. Zhao, C. Liu and B. Zhang, *Nat. Catal.*, 2023, **6**, 906–915.

56 J. Xian, S. Li, H. Su, P. Liao, S. Wang, R. Xiang, Y. Zhang, Q. Liu and G. Li, *Angew. Chem., Int. Ed.*, 2023, **62**, e202306726.

57 S. Shin, S. Sultan, Z.-X. Chen, H. Lee, H. Choi, T.-U. Wi, C. Park, T. Kim, C. Lee, J. Jeong, H. Shin, T.-H. Kim, H. Ju, H. C. Yoon, H.-K. Song, H.-W. Lee, M.-J. Cheng and Y. Kwon, *Energy Environ. Sci.*, 2023, **16**, 2003–2013.

58 Y. Luo, K. Xie, P. Ou, C. Lavallais, T. Peng, Z. Chen, Z. Zhang, N. Wang, X.-Y. Li, I. Grigioni, B. Liu, D. Sinton, J. B. Dunn and E. H. Sargent, *Nat. Catal.*, 2023, **6**, 939–948.

59 M. Xu, F. Wu, Y. Zhang, Y. Yao, G. Zhu, X. Li, L. Chen, G. Jia, X. Wu, Y. Huang, P. Gao and W. Ye, *Nat. Commun.*, 2023, **14**, 6994.

60 J. E. Kim, J. H. Jang, K. M. Lee, M. Balamurugan, Y. I. Jo, M. Y. Lee, S. Choi, S. W. Im and K. T. Nam, *Angew. Chem., Int. Ed.*, 2021, **60**, 21943–21951.

61 C. Guo, W. Zhou, X. Lan, Y. Wang, T. Li, S. Han, Y. Yu and B. Zhang, *J. Am. Chem. Soc.*, 2022, **144**, 16006–16011.

62 J. Lan, Z. Wei, Y.-R. Lu, D. Chen, S. Zhao, T.-S. Chan and Y. Tan, *Nat. Commun.*, 2023, **14**, 2870.

63 Y. Feng, H. Yang, Y. Zhang, X. Huang, L. Li, T. Cheng and Q. Shao, *Nano Lett.*, 2020, **20**, 8282–8289.

64 N. Meng, Y. Huang, Y. Liu, Y. Yu and B. Zhang, *Cell Rep. Phys. Sci.*, 2021, **2**, 100378.

65 D. Saravanakumar, J. Song, S. Lee, N. H. Hur and W. Shin, *ChemSusChem*, 2017, **10**, 3999–4003.

66 N. Cao, Y. Quan, A. Guan, C. Yang, Y. Ji, L. Zhang and G. Zheng, *J. Colloid Interface Sci.*, 2020, **577**, 109–114.

67 Z. Tao, Y. Wu, Z. Wu, B. Shang, C. Rooney and H. Wang, *J. Energy Chem.*, 2022, **65**, 367–370.

68 R. J. Lewis, K. Ueura, X. Liu, Y. Fukuta, T. E. Davies, D. J. Morgan, L. Chen, J. Qi, J. Singleton, J. K. Edwards, S. J. Freakley, C. J. Kiely, Y. Yamamoto and G. J. Hutchings, *Science*, 2022, **376**, 615–620.

69 G. R. Tauszik and P. Crocetta, *Appl. Catal.*, 1985, **17**, 1–21.

70 R. J. Lewis, K. Ueura, X. Liu, Y. Fukuta, T. Qin, T. E. Davies, D. J. Morgan, A. Stenner, J. Singleton, J. K. Edwards, S. J. Freakley, C. J. Kiely, L. Chen, Y. Yamamoto and G. J. Hutchings, *ACS Catal.*, 2023, **13**, 1934–1945.

71 A. Thangaraj, S. Sivasanker and P. Ratnasamy, *J. Catal.*, 1991, **131**, 394–400.

72 Y. Wu, C. Liu, C. Wang, Y. Yu, Y. Shi and B. Zhang, *Nat. Commun.*, 2021, **12**, 3881.

73 R. Xiang, S. Wang, P. Liao, F. Xie, J. Kang, S. Li, J. Xian, L. Guo and G. Li, *Angew. Chem., Int. Ed.*, 2023, **62**, e202312239.

74 D. P. Butcher and A. A. Gewirth, *Nano Energy*, 2016, **29**, 457–465.

75 T. J. Hager and L. R. Sadergaski, *Measuring Hydroxylammonium, Nitrate, and Nitrite Concentration with Raman Spectroscopy for ^{238}Pu Supply Program*, 2021.

76 J. Zhou, S. Han, R. Yang, T. Li, W. Li, Y. Wang, Y. Yu and B. Zhang, *Angew. Chem., Int. Ed.*, 2023, **62**, e202305184.

77 Y. Huang, C. He, C. Cheng, S. Han, M. He, Y. Wang, N. Meng, B. Zhang, Q. Lu and Y. Yu, *Nat. Commun.*, 2023, **14**, 7368.

78 P. Li, R. Li, Y. Liu, M. Xie, Z. Jin and G. Yu, *J. Am. Chem. Soc.*, 2023, **145**, 6471–6479.

79 M. He, Y. Wu, R. Li, Y. Wang, C. Liu and B. Zhang, *Nat. Commun.*, 2023, **14**, 5088.

80 T. Burdyny and W. A. Smith, *Energy Environ. Sci.*, 2019, **12**, 1442–1453.

81 C. T. Dinh, T. Burdyny, M. G. Kibria, A. Seifitokaldani, C. M. Gabardo, F. P. G. de Arquer, A. Kiani, J. P. Edwards, P. De Luna, O. S. Bushuyev, C. Q. Zou, R. Quintero-Bermudez, Y. J. Pang, D. Sinton and E. H. Sargent, *Science*, 2018, **360**, 783–787.

82 D. Gao, R. M. Arán-Ais, H. S. Jeon and B. Roldan Cuenya, *Nat. Catal.*, 2019, **2**, 198–210.

83 T. Li, E. W. Lees, M. Goldman, D. A. Salvatore, D. M. Weekes and C. P. Berlinguette, *Joule*, 2019, **3**, 1487–1497.

84 T. Li, E. W. Lees, Z. S. Zhang and C. P. Berlinguette, *ACS Energy Lett.*, 2020, **5**, 2624–2630.

85 J. He, A. Huang, N. J. J. Johnson, K. E. Dettelbach, D. M. Weekes, Y. Cao and C. P. Berlinguette, *Inorg. Chem.*, 2018, **57**, 14624–14631.

86 Y. Hori, H. Konishi, T. Futamura, A. Murata, O. Koga, H. Sakurai and K. Oguma, *Electrochim. Acta*, 2005, **50**, 5354–5369.

87 G. Pérez, R. Ibáñez, A. M. Urtiaga and I. Ortiz, *Chem. Eng. J.*, 2012, **197**, 475–482.

88 X. Ma, M. Li, C. Feng and Z. He, *J. Hazard. Mater.*, 2020, **388**, 122085.

89 Y. Zhang, Y. Zhao, Z. Chen, L. Wang, P. Wu and F. Wang, *Electrochim. Acta*, 2018, **291**, 151–160.